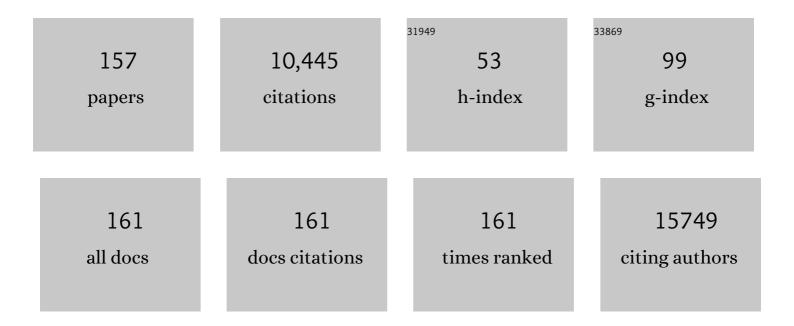
List of Publications by Year in descending order

Source: https://exaly.com/author-pdf/5023362/publications.pdf Version: 2024-02-01



#	Article	IF	CITATIONS
1	Strong polarization enhancement in asymmetric three-component ferroelectric superlattices. Nature, 2005, 433, 395-399.	13.7	627
2	pâ€ŧype ZnSe by nitrogen atom beam doping during molecular beam epitaxial growth. Applied Physics Letters, 1990, 57, 2127-2129.	1.5	622
3	Synthesis of Novel Thin-Film Materials by Pulsed Laser Deposition. Science, 1996, 273, 898-903.	6.0	547
4	PdSe <sub>2</sub> : Pentagonal Two-Dimensional Layers with High Air Stability for Electronics. Journal of the American Chemical Society, 2017, 139, 14090-14097.	6.6	509
5	Nanoscale effects on the ionic conductivity in highly textured YSZ thin films. Solid State Ionics, 2005, 176, 1319-1326.	1.3	330
6	2D/2D heterojunction of Ti <sub>3</sub> C <sub>2</sub> /g-C <sub>3</sub> N <sub>4</sub> nanosheets for enhanced photocatalytic hydrogen evolution. Nanoscale, 2019, 11, 8138-8149.	2.8	289
7	High-Performance Flexible Perovskite Solar Cells by Using a Combination of Ultrasonic Spray-Coating and Low Thermal Budget Photonic Curing. ACS Photonics, 2015, 2, 680-686.	3.2	268
8	Interlayer Coupling in Twisted WSe <sub>2</sub> /WS <sub>2</sub> Bilayer Heterostructures Revealed by Optical Spectroscopy. ACS Nano, 2016, 10, 6612-6622.	7.3	249
9	Perovskite Solar Cells with Near 100% Internal Quantum Efficiency Based on Large Single Crystalline Grains and Vertical Bulk Heterojunctions. Journal of the American Chemical Society, 2015, 137, 9210-9213.	6.6	246
10	Two-dimensional GaSe/MoSe <sub>2</sub> misfit bilayer heterojunctions by van der Waals epitaxy. Science Advances, 2016, 2, e1501882.	4.7	239
11	Ultrathin nanosheets of CrSiTe <sub>3</sub> : a semiconducting two-dimensional ferromagnetic material. Journal of Materials Chemistry C, 2016, 4, 315-322.	2.7	235
12	Controlled Vapor Phase Growth of Single Crystalline, Two-Dimensional GaSe Crystals with High Photoresponse. Scientific Reports, 2014, 4, 5497.	1.6	222
13	Patterned arrays of lateral heterojunctions within monolayer two-dimensional semiconductors. Nature Communications, 2015, 6, 7749.	5.8	213
14	Monolayer Ti <sub>3</sub> C <sub>2</sub> <i>T</i> <sub><i>x</i></sub> as an Effective Co-catalyst for Enhanced Photocatalytic Hydrogen Production over TiO <sub>2</sub> . ACS Applied Energy Materials, 2019, 2, 4640-4651.	2.5	177
15	Nature of the band gap and origin of the electro-/photo-activity of Co3O4. Journal of Materials Chemistry C, 2013, 1, 4628.	2.7	176
16	Structure and Formation Mechanism of Black TiO <sub>2</sub> Nanoparticles. ACS Nano, 2015, 9, 10482-10488.	7.3	170
17	The Role of Ru Redox in pH-Dependent Oxygen Evolution on Rutile Ruthenium Dioxide Surfaces. CheM, 2017, 2, 668-675.	5.8	151
18	Functionally graded hydroxyapatite coatings doped with antibacterial components. Acta Biomaterialia, 2010, 6, 2264-2273.	4.1	143

2

#	Article	IF	CITATIONS
19	Low Energy Implantation into Transition-Metal Dichalcogenide Monolayers to Form Janus Structures. ACS Nano, 2020, 14, 3896-3906.	7.3	136
20	Antioxidant Deactivation on Graphenic Nanocarbon Surfaces. Small, 2011, 7, 2775-2785.	5.2	133
21	Thickness-dependent charge transport in few-layer MoS <sub>2</sub> field-effect transistors. Nanotechnology, 2016, 27, 165203.	1.3	124
22	Tailoring Vacancies Far Beyond Intrinsic Levels Changes the Carrier Type and Optical Response in Monolayer MoSe <sub>2â^'<i>x</i></sub> Crystals. Nano Letters, 2016, 16, 5213-5220.	4.5	121
23	Carbon Nanotubes Grown on Metal Microelectrodes for the Detection of Dopamine. Analytical Chemistry, 2016, 88, 645-652.	3.2	113
24	PSâ€ <i>b</i> â€₽3HT Copolymers as P3HT/PCBM Interfacial Compatibilizers for High Efficiency Photovoltaics. Advanced Materials, 2011, 23, 5529-5535.	11.1	110
25	Pulsed Laser Deposition of Photoresponsive Twoâ€Dimensional GaSe Nanosheet Networks. Advanced Functional Materials, 2014, 24, 6365-6371.	7.8	108
26	Excimer laser reduction and patterning of graphite oxide. Carbon, 2013, 53, 81-89.	5.4	107
27	The isotopic effects of deuteration on optoelectronic properties of conducting polymers. Nature Communications, 2014, 5, 3180.	5.8	103
28	Van der Waals Epitaxial Growth of Two-Dimensional Single-Crystalline GaSe Domains on Graphene. ACS Nano, 2015, 9, 8078-8088.	7.3	103
29	Ultrafast Charge Transfer and Hybrid Exciton Formation in 2D/0D Heterostructures. Journal of the American Chemical Society, 2016, 138, 14713-14719.	6.6	102
30	In situ edge engineering in two-dimensional transition metal dichalcogenides. Nature Communications, 2018, 9, 2051.	5.8	100
31	Deciphering Halogen Competition in Organometallic Halide Perovskite Growth. Journal of the American Chemical Society, 2016, 138, 5028-5035.	6.6	92
32	Cooperative Island Growth of Large-Area Single-Crystal Graphene on Copper Using Chemical Vapor Deposition. ACS Nano, 2014, 8, 5657-5669.	7.3	91
33	Isoelectronic Tungsten Doping in Monolayer MoSe <sub>2</sub> for Carrier Type Modulation. Advanced Materials, 2016, 28, 8240-8247.	11.1	85
34	Suppression of Defects and Deep Levels Using Isoelectronic Tungsten Substitution in Monolayer MoSe <sub>2</sub> . Advanced Functional Materials, 2017, 27, 1603850.	7.8	84
35	Defect-Mediated Phase Transformation in Anisotropic Two-Dimensional PdSe <sub>2</sub> Crystals for Seamless Electrical Contacts. Journal of the American Chemical Society, 2019, 141, 8928-8936.	6.6	81
36	Twoâ€Dimensional Palladium Diselenide with Strong Inâ€Plane Optical Anisotropy and High Mobility Grown by Chemical Vapor Deposition. Advanced Materials, 2020, 32, e1906238.	11.1	81

#	Article	IF	CITATIONS
37	A water-soluble polythiophene for organic field-effect transistors. Polymer Chemistry, 2013, 4, 5270.	1.9	78
38	Surface/Interface-Related Conductivity in Nanometer Thick YSZ Films. Electrochemical and Solid-State Letters, 2004, 7, A459.	2.2	76
39	Growth control of oxygen stoichiometry in homoepitaxial SrTiO3 films by pulsed laser epitaxy in high vacuum. Scientific Reports, 2016, 6, 19941.	1.6	75
40	Thermal stability of epitaxial SrRuO3 films as a function of oxygen pressure. Applied Physics Letters, 2004, 84, 4107-4109.	1.5	71
41	Superconducting magnesium diboride films with Tcâ‰^24 K grown by pulsed laser deposition with in situ anneal. Physica C: Superconductivity and Its Applications, 2001, 353, 157-161.	0.6	69
42	Metal-assisted hydrogen storage on Pt-decorated single-walled carbon nanohorns. Carbon, 2012, 50, 4953-4964.	5.4	69
43	Single walled carbon nanohorns as photothermal cancer agents. Lasers in Surgery and Medicine, 2011, 43, 43-51.	1.1	67
44	Edge-Controlled Growth and Etching of Two-Dimensional GaSe Monolayers. Journal of the American Chemical Society, 2017, 139, 482-491.	6.6	65
45	Blue photoluminescence in ZnGa[sub 2]O[sub 4] thin-film phosphors. Journal of Applied Physics, 2001, 89, 1653.	1.1	63
46	Real-time imaging of vertically aligned carbon nanotube array growth kinetics. Nanotechnology, 2008, 19, 055605.	1.3	61
47	UV-activated ZnO films on a flexible substrate for room temperature O2 and H2O sensing. Scientific Reports, 2017, 7, 6053.	1.6	61
48	Realâ€Time Observation of Orderâ€Disorder Transformation of Organic Cations Induced Phase Transition and Anomalous Photoluminescence in Hybrid Perovskites. Advanced Materials, 2018, 30, e1705801.	11.1	60
49	Time-resolved study of SrTiO3 homoepitaxial pulsed-laser deposition using surface x-ray diffraction. Applied Physics Letters, 2002, 80, 3379-3381.	1.5	59
50	Model for Self-Assembly of Carbon Nanotubes from Acetylene Based on Real-Time Studies of Vertically Aligned Growth Kinetics. Journal of Physical Chemistry C, 2009, 113, 15484-15491.	1.5	59
51	Vacuum-Assisted Low-Temperature Synthesis of Reduced Graphene Oxide Thin-Film Electrodes for High-Performance Transparent and Flexible All-Solid-State Supercapacitors. ACS Applied Materials & Interfaces, 2018, 10, 11008-11017.	4.0	57
52	Germanium-Catalyzed Growth of Zinc Oxide Nanowires: A Semiconductor Catalyst for Nanowire Synthesis. Angewandte Chemie - International Edition, 2005, 44, 274-278.	7.2	56
53	In Vitro and in Vivo Studies of Single-Walled Carbon Nanohorns with Encapsulated Metallofullerenes and Exohedrally Functionalized Quantum Dots. Nano Letters, 2010, 10, 2843-2848.	4.5	56
54	Observation of Nanoscale Morphological and Structural Degradation in Perovskite Solar Cells by in Situ TEM. ACS Applied Materials & Interfaces, 2016, 8, 32333-32340.	4.0	54

#	Article	IF	CITATIONS
55	Silicon and zinc telluride nanoparticles synthesized by pulsed laser ablation: size distributions and nanoscale structure. Applied Surface Science, 1998, 127-129, 355-361.	3.1	51
56	An improved continuous compositional-spread technique based on pulsed-laser deposition and applicable to large substrate areas. Review of Scientific Instruments, 2003, 74, 4058-4062.	0.6	49
57	Continuous composition-spread thin films of transition metal oxides by pulsed-laser deposition. Applied Surface Science, 2004, 223, 35-38.	3.1	49
58	Atomic Layer Engineering of Perovskite Oxides for Chemically Sharp Heterointerfaces. Advanced Materials, 2012, 24, 6423-6428.	11.1	49
59	Silicon and zinc telluride nanoparticles synthesized by low energy density pulsed laser ablation into ambient gases. Journal of Materials Research, 1999, 14, 359-370.	1.2	48
60	Digital Transfer Growth of Patterned 2D Metal Chalcogenides by Confined Nanoparticle Evaporation. ACS Nano, 2014, 8, 11567-11575.	7.3	47
61	Nonequilibrium Interlayer Transport in Pulsed Laser Deposition. Physical Review Letters, 2006, 96, 226104.	2.9	46
62	Low thermal budget, photonic-cured compact TiO <sub>2</sub> layers for high-efficiency perovskite solar cells. Journal of Materials Chemistry A, 2016, 4, 9685-9690.	5.2	46
63	Strain tolerance of two-dimensional crystal growth on curved surfaces. Science Advances, 2019, 5, eaav4028.	4.7	46
64	Revealing the Preferred Interlayer Orientations and Stackings of Twoâ€Dimensional Bilayer Gallium Selenide Crystals. Angewandte Chemie - International Edition, 2015, 54, 2712-2717.	7.2	45
65	Observation of two distinct negative trions in tungsten disulfide monolayers. Physical Review B, 2015, 92, .	1.1	44
66	GaAs substrate cleaning for epitaxy using a remotely generated atomic hydrogen beam. Journal of Applied Physics, 1993, 73, 4610-4613.	1.1	42
67	Nanoparticle generation and transport resulting from femtosecond laser ablation of ultrathin metal films: Time-resolved measurements and molecular dynamics simulations. Applied Physics Letters, 2014, 104, .	1.5	42
68	Ultrafast Dynamics of Metal Plasmons Induced by 2D Semiconductor Excitons in Hybrid Nanostructure Arrays. ACS Photonics, 2016, 3, 2389-2395.	3.2	42
69	Isotope-Engineering the Thermal Conductivity of Two-Dimensional MoS <sub>2</sub> . ACS Nano, 2019, 13, 2481-2489.	7.3	42
70	Pulsed Growth of Vertically Aligned Nanotube Arrays with Variable Density. ACS Nano, 2010, 4, 7573-7581.	7.3	41
71	Controllable Growth of Perovskite Films by Roomâ€Temperature Air Exposure for Efficient Planar Heterojunction Photovoltaic Cells. Angewandte Chemie - International Edition, 2015, 54, 14862-14865.	7.2	41
72	The Influence of Local Distortions on Proton Mobility in Acceptor Doped Perovskites. Chemistry of Materials, 2018, 30, 4919-4925.	3.2	40

#	Article	IF	CITATIONS
73	Intrinsic Defects in MoS <sub>2</sub> Grown by Pulsed Laser Deposition: From Monolayers to Bilayers. ACS Nano, 2021, 15, 2858-2868.	7.3	40
74	Growth of highly doped pâ€ŧype ZnTe films by pulsed laser ablation in molecular nitrogen. Applied Physics Letters, 1995, 67, 2545-2547.	1.5	38
75	Magnetic order multilayering in FeRh thin films by He-Ion irradiation. Materials Research Letters, 2018, 6, 106-112.	4.1	36
76	Cumulative and continuous laser vaporization synthesis of single wall carbon nanotubes and nanohorns. Applied Physics A: Materials Science and Processing, 2008, 93, 849-855.	1.1	34
77	Flux-Dependent Growth Kinetics and Diameter Selectivity in Single-Wall Carbon Nanotube Arrays. ACS Nano, 2011, 5, 8311-8321.	7.3	33
78	Nonequilibrium Synthesis of TiO <sub>2</sub> Nanoparticle "Building Blocks―for Crystal Growth by Sequential Attachment in Pulsed Laser Deposition. Nano Letters, 2017, 17, 4624-4633.	4.5	33
79	Growth of p-type ZnTe and n-type CdSe films on GaAs(001) by pulsed laser ablation. Applied Surface Science, 1998, 127-129, 418-424.	3.1	32
80	High-throughput growth temperature optimization of ferroelectric SrxBa1â^'xNb2O6 epitaxial thin films using a temperature gradient method. Applied Physics Letters, 2004, 84, 1350-1352.	1.5	31
81	Transmission two-modulator generalized ellipsometry measurements. Applied Optics, 2002, 41, 6555.	2.1	29
82	Low temperature synthesis of hierarchical TiO <sub>2</sub> nanostructures for high performance perovskite solar cells by pulsed laser deposition. Physical Chemistry Chemical Physics, 2016, 18, 27067-27072.	1.3	29
83	Normal-incidence generalized ellipsometry using the two-modulator generalized ellipsometry microscope. Applied Optics, 2006, 45, 5479.	2.1	25
84	Pulsed laser CVD investigations of single-wall carbon nanotube growth dynamics. Applied Physics A: Materials Science and Processing, 2008, 93, 987-993.	1.1	25
85	An integrated portable Raman sensor with nanofabricated gold bowtie array substrates for energetics detection. Analyst, The, 2011, 136, 1697.	1.7	25
86	Speciation and Electronic Structure of La1â^'xSrxCoO3â^'δ During Oxygen Electrolysis. Topics in Catalysis, 2018, 61, 2161-2174.	1.3	25
87	Designing Morphotropic Phase Composition in BiFeO <sub>3</sub> . Nano Letters, 2019, 19, 1033-1038.	4.5	24
88	Fluorination of "brick and mortar―soft-templated graphitic ordered mesoporous carbons for high power lithium-ion battery. Journal of Materials Chemistry A, 2013, 1, 9414.	5.2	23
89	Uniform, Homogenous Coatings of Carbon Nanohorns on Arbitrary Substrates from Common Solvents. ACS Applied Materials & Interfaces, 2013, 5, 13153-13160.	4.0	23
90	Bottom up synthesis of boron-doped graphene for stable intermediate temperature fuel cell electrodes. Carbon, 2017, 123, 605-615.	5.4	23

#	Article	IF	CITATIONS
91	A Facile High-speed Vibration Milling Method to Water-disperse Single-walled Carbon Nanohorns. Chemistry of Materials, 2010, 22, 347-351.	3.2	22
92	Real-time optical diagnostics of graphene growth induced by pulsed chemical vapor deposition. Nanoscale, 2013, 5, 6507.	2.8	22
93	The growth and assembly of organic molecules and inorganic 2D materials on graphene for van der Waals heterostructures. Carbon, 2018, 131, 246-257.	5.4	21
94	Strain-free, ultra-high purity ZnSe layers grown by molecular beam epitaxy. Journal of Materials Research, 1990, 5, 475-477.	1.2	20
95	Influence of MgO substrate miscut on domain structure of pulsed laser deposited SrxBa1â^'xNb2O6 as characterized by x-ray diffraction and spectroscopic ellipsometry. Applied Physics Letters, 2003, 82, 2990-2992.	1.5	20
96	A laser-deposition approach to compositional-spread discovery of materials on conventional sample sizes. Measurement Science and Technology, 2005, 16, 21-31.	1.4	20
97	Anomalous Oxidation States in Multilayers for Fuel Cell Applications. Advanced Functional Materials, 2010, 20, 2664-2674.	7.8	20
98	Persistent photoconductivity in two-dimensional Mo <sub>1â^'<i>x</i></sub> W <sub><i>x</i></sub> Se <sub>2</sub> –MoSe <sub>2</sub> van der Waals heterojunctions. Journal of Materials Research, 2016, 31, 923-930.	1.2	20
99	Pulsed electron deposition of fluorine-based precursors for YBa2Cu3O7â^'x-coated conductors. Superconductor Science and Technology, 2005, 18, 1168-1175.	1.8	19
100	Strain-Induced Growth of Twisted Bilayers during the Coalescence of Monolayer MoS <sub>2</sub> Crystals. ACS Nano, 2021, 15, 4504-4517.	7.3	19
101	Amorphous Diamond Films Deposited by Pulsed-Laser Ablation: the Optimum Carbon-Ion Kinetic Energy and Effects of Laser Wavelength. Materials Research Society Symposia Proceedings, 1998, 526, 325.	0.1	18
102	In situ timeâ€resolved measurements of carbon nanotube and nanohorn growth. Physica Status Solidi (B): Basic Research, 2007, 244, 3944-3949.	0.7	18
103	Influence of Nonstoichiometry on Proton Conductivity in Thin-Film Yttrium-Doped Barium Zirconate. ACS Applied Materials & Interfaces, 2018, 10, 4816-4823.	4.0	18
104	Revealing the surface and bulk regimes of isothermal graphene nucleation and growth on Ni with in situ kinetic measurements and modeling. Carbon, 2014, 79, 256-264.	5.4	16
105	Dislocations in latticeâ€mismatched wideâ€gap IIâ€VI/GaAs heterostructures as laser light scatterers: Experiment and theory. Journal of Applied Physics, 1995, 78, 1203-1209.	1.1	15
106	Growth of oxide seed layers on ni and other technologically interesting metal substrates: issues related to formation and control of sulfur superstructures for texture optimization. IEEE Transactions on Applied Superconductivity, 2003, 13, 2646-2650.	1.1	15
107	Quantitative determination of energy enhanced interlayer transport in pulsed laser deposition of SrTiO3. Physical Review B, 2011, 84, .	1.1	15
108	Black Anatase Formation by Annealing of Amorphous Nanoparticles and the Role of the Ti <sub>2</sub> O <sub>3</sub> Shell in Self-Organized Crystallization by Particle Attachment. ACS Applied Materials & Interfaces, 2017, 9, 22018-22025.	4.0	15

#	Article	IF	CITATIONS
109	Determination of optical birefringence by using off-axis transmission ellipsometry. Applied Optics, 2005, 44, 3153.	2.1	14
110	Spatial and temporal measurements of temperature and cell viability in response to nanoparticle-mediated photothermal therapy. Nanomedicine, 2012, 7, 1729-1742.	1.7	14
111	Anorthite sputtering by H <sup>+</sup> and Ar <sup><i>q</i>+</sup> ( <i>q</i> = 1–9) at solar wind velocities. Journal of Geophysical Research: Space Physics, 2014, 119, 8006-8016.	0.8	14
112	In situ laser reflectivity to monitor and control the nucleation and growth of atomically thin 2D materials*. 2D Materials, 2020, 7, 025048.	2.0	14
113	Selective Antisite Defect Formation in WS <sub>2</sub> Monolayers via Reactive Growth on Dilute Wâ€Au Alloy Substrates. Advanced Materials, 2022, 34, e2106674.	11.1	14
114	Stabilized Synthesis of 2D Verbeekite: Monoclinic PdSe <sub>2</sub> Crystals with High Mobility and In-Plane Optical and Electrical Anisotropy. ACS Nano, 2022, 16, 13900-13910.	7.3	14
115	In situ, realâ€ŧime diffuse optical reflectivity measurements during GaAs cleaning and subsequent ZnSe/GaAs heteroepitaxy. Journal of Vacuum Science and Technology A: Vacuum, Surfaces and Films, 1993, 11, 1792-1795.	0.9	13
116	Interfaces in perovskite heterostructures. Applied Physics A: Materials Science and Processing, 2008, 93, 807-811.	1.1	12
117	Nanostructured carbon electrocatalyst supports for intermediate-temperature fuel cells: Single-walled versus multi-walled structures. Journal of Power Sources, 2017, 337, 145-151.	4.0	12
118	Investigating local oxidation processes in Fe thin films in a water vapor environment by in situ liquid cell TEM. Ultramicroscopy, 2020, 209, 112842.	0.8	11
119	Insiturealâ€ŧime determination of the freeâ€carrier density in doped ZnSe films during molecular beam epitaxial growth. Applied Physics Letters, 1992, 60, 2723-2725.	1.5	10
120	High-temperature transformation of Fe-decorated single-wall carbon nanohorns to nanooysters: a combined experimental and theoretical study. Nanoscale, 2013, 5, 1849-1857.	2.8	10
121	Self-Powered Fast Brazing of Ti-6Al-4V Using Ni/Al Reactive Multilayer Films. Applied Sciences (Switzerland), 2018, 8, 985.	1.3	10
122	Low-Temperature Charging Dynamics of the Ionic Liquid and Its Gating Effect on FeSe <sub>0.5</sub> Te <sub>0.5</sub> Superconducting Films. ACS Applied Materials & Interfaces, 2019, 11, 17979-17986.	4.0	10
123	Heteroepitaxial growth of n-type CdSe on GaAs(001) by pulsed laser deposition: studies of film–substrate interdiffusion and indium diffusion. Journal of Crystal Growth, 1998, 193, 516-527.	0.7	9
124	R&D of RABiTS-based coated conductors: Conversion of ex situ YBCO superconductor using a novel pulsed electron-beam deposited precursor. Physica C: Superconductivity and Its Applications, 2005, 426-431, 878-886.	0.6	9
125	Incremental Growth of Short SWNT Arrays by Pulsed Chemical Vapor Deposition. Small, 2012, 8, 1534-1542.	5.2	9
126	Altering the catalytic activity of thin metal catalyst films forÂcontrolled growth of chemical vapor deposited vertically aligned carbon nanotube arrays. Applied Physics A: Materials Science and Processing, 2008, 93, 1005-1009.	1.1	8

#	Article	IF	CITATIONS
127	Narrow and intense resonances in the low-frequency region of surface-enhanced Raman spectra of single-wall carbon nanotubes. Physical Review B, 2010, 82, .	1.1	8
128	Layer-by-layer epitaxial thin films of the pyrochlore Tb <sub>2</sub> Ti <sub>2</sub> O <sub>7</sub> . Nanotechnology, 2017, 28, 055708.	1.3	8
129	In Quest of a Ferromagnetic Insulator: Structure-Controlled Magnetism in Mg–Ti–O Thin Films. Journal of Physical Chemistry C, 2019, 123, 19970-19978.	1.5	8
130	Epitaxial Growth and Luminescent Properties of Mn2+-Activated ZnGa2O4 Films. , 2000, 4, 293-297.		7
131	Roomâ€Temperature Insulating Ferromagnetic (Ni,Co) 1+2 x Ti 1â^' x O 3 Thin Films. Annalen Der Physik, 2019, 531, 1900299.	0.9	7
132	Understanding Substrate-Guided Assembly in van der Waals Epitaxy by <i>in Situ</i> Laser Crystallization within a Transmission Electron Microscope. ACS Nano, 2021, 15, 8638-8652.	7.3	7
133	Pulsed KrF laser deposited GaN/TiN/Si(111) heterostructures by sequential TiN and liquid Ga laser ablation. Applied Physics A: Materials Science and Processing, 1999, 69, S441-S445.	1.1	6
134	Slowing of femtosecond laser-generated nanoparticles in a background gas. Applied Physics Letters, 2014, 105, 213108.	1.5	6
135	Substoichiometric Tuning of the Electronic Properties of Titania. Thin Solid Films, 2021, 717, 138437.	0.8	6
136	Revealing the Preferred Interlayer Orientations and Stackings of Twoâ€Dimensional Bilayer Gallium Selenide Crystals. Angewandte Chemie, 2015, 127, 2750-2755.	1.6	5
137	Vacancy filled nickelâ€cobaltâ€titanate thin films. Physica Status Solidi (B): Basic Research, 2017, 254, 1600799.	0.7	5
138	Unusual electrical conductivity driven by localized stoichiometry modification at vertical epitaxial interfaces. Materials Horizons, 2020, 7, 3217-3225.	6.4	5
139	Pulsed Laser Ablation Growth and Doping of Epitaxial Compound Semiconductor Films. Materials Research Society Symposia Proceedings, 1995, 397, 107.	0.1	4
140	p-type ZnSe : N grown by molecular beam epitaxy: evidence of non-radiative recombination centers in moderately to heavily doped material. Journal of Crystal Growth, 1994, 138, 352-356.	0.7	3
141	Study of Substrate Diffusion in Epitaxial N-Type CdSe Films Grown on GaAs (001) by Pulsed Laser Ablation. Materials Research Society Symposia Proceedings, 1998, 526, 27.	0.1	3
142	The use of low-energy SIMS (LE-SIMS) for nanoscale fuel cell material development. Surface and Interface Analysis, 2011, 43, 635-638.	0.8	3
143	Stabilizing Ir(001) Epitaxy on Yttria-Stabilized Zirconia Using a Thin Ir Seed Layer Grown by Pulsed Laser Deposition. Crystal Growth and Design, 2017, 17, 89-94.	1.4	3
144	Exploring the Spatial Control of Topotactic Phase Transitions Using Vertically Oriented Epitaxial Interfaces. Nano-Micro Letters, 2022, 14, 2.	14.4	3

#	Article	IF	CITATIONS
145	Design and implementation of a magnetic drive retrofit to the Vacuum Generator's venetian style viewport shutter assembly. Journal of Vacuum Science and Technology A: Vacuum, Surfaces and Films, 1993, 11, 464-465.	0.9	2
146	Characterization of linear diattenuator and retarders using a two-modulator generalized ellipsometer (2-MGE). , 2002, , .		2
147	Generalized ellipsometry in unusual configurations. Applied Surface Science, 2006, 253, 47-51.	3.1	2
148	Catalytic nanoparticles for carbon nanotube growth synthesized by through thin film femtosecond laser ablation. Proceedings of SPIE, 2014, , .	0.8	1
149	Growth of Highly Doped P-Type Znte Films by Pulsed Laser ablation in Molecular Nitrogen. Materials Research Society Symposia Proceedings, 1995, 388, 85.	0.1	0
150	ZnGa2O4 Thin-Film Phosphors Grown by Pulsed Laser Ablation. Materials Research Society Symposia Proceedings, 1999, 560, 59.	0.1	0
151	Spectroscopic Ellipsometry Studies of Nanocrystalline Silicon in Thin-Film Silicon Dioxide. Materials Research Society Symposia Proceedings, 2002, 737, 319.	0.1	0
152	Nanoengineering: Atomic Layer Engineering of Perovskite Oxides for Chemically Sharp Heterointerfaces (Adv. Mater. 48/2012). Advanced Materials, 2012, 24, 6422-6422.	11.1	0
153	Nonequilibrium laser synthesis and real-time diagnostics of carbon nanomaterial growth. , 2012, , .		0
154	Exploring growth kinetics of carbon nanotube arrays by in situ optical diagnostics and modeling. Proceedings of SPIE, 2014, , .	0.8	0
155	Preparation of Thick Ni/Al Reactive Multilayer Films and Prospective Use for Self-Powered Brazing of Ti-6Al-4V. , 2018, , .		0
156	Permanently Magnetized Insulating Thinâ€Film Devices by Reduction. Physica Status Solidi - Rapid Research Letters, 2020, 14, 2000346.	1.2	0
157	Simulation of the Impact of Point Defects and Edge Dislocations on Xâ€Ray Diffraction in Hexagonal (Ni,Co) <sub> 1+2 <i>x</i> </sub> Ti <sub> 1â^' <i>x</i> </sub> O <sub>3</sub> Thin Films. Physica Status Solidi (B): Basic Research, 0, , 2100583.	0.7	0